# Proportional Mode Calorimeters of the TPC Facility

C.D.Buchanan, M.Chronoviat, J.M.Hauptman, R.I.Koda, J.Kubic,
D.Park, J.Spahn, D.H.Stork, W.E.Slater, H.K.Ticho,
M.Wayne, R.van Daalen Wetters
Department of Physics, University of California
Los Angeles, California 90024

M.Alston-Garnjost, A.Barbaro-Galtieri, A.V.Barnes, A.Bross,
W.C.Carithers, O.Chamberlain, A.R.Clark, O.I.Dahl, C.T.Day,
P.Delpierre, K.A.Derby, P.H.Eberhard, D.L.Fancher, B.Gabioud,
J.W.Gary, N.J.Hadley, B.Heck, H.J.Hilke, W.Hofmann, J.E.Huth,
H.Iwasaki, R.W.Kenney, L.T.Kerth, S.C.Loken, G.W.London,
G.R.Lynch, R.J.Madaras, R.Majka, J.Mallet, P.S.Martin,
J.N.Marx, W.Moses, P.Nemethy, D.R.Nygren, P.J.Oddone, M.Pripstein,
P.R.Robrish, M.T.Ronan, R.R.Ross, F.R.Rouse, G.Shapiro, M.D.Shapiro,
M.L.Stevenson, M.Urban, R.van Tyen, H.Videau, W.A.Wenzel
Lawrence Berkeley Laboratory, Berkeley, California 94720

W.Gorn, K.K.Kwong, J.G.Layter, C.S.Lindsey,
S.O.Melnikoff, B.C.Shen, G.J.VanDalen,
University of California, Riverside, California 92521

D.H.Badtke, J.A.Bakken, B.A.Barnett, B.Blumenfeld, C-Y.Chien,
J.Hylen, L.Madansky, J.A.J.Matthews, A.Pevsner, W-M.Zhang
Johns Hopkins University, Baltimore, Maryland 21218

H.Aihara, J.Chiba, H.Fujii, T.Fujii, T.Kamae,
K.Maruyama, N.Toge, M.Yamauchi
University of Tokyo, Tokyo, Japan

R.R.Kofler, M.E.Zeller
Yale University, New Haven, Connecticut 06520

## Abstract

Two wire proportional mode gas calorimeter modules have been tested as prototypes for the Pole Tip calorimeters of the TPC Facility at PEP. The results of the tests at several electron energies (0.25 to 12. GeV) and several pressures (1.0 to 30. atms) are presented, comparisons with a detailed simulation program are made, and results from the Pole Tip modules now operating at PEP are given.

## Introduction

The TPC Facility at PEP has over 90% solid angle coverage by fine-grained electromagnetic calorimeters. The barrel Geiger mode device is described by Wenzel[1] at this Workshop. The end cap calorimeters are proportional mode devices. Studies utilized in their design are described in this paper. Gaseous proportional mode was chosen for the Pole Tips since these calorimeters must use the TPC gas mixture of 80% Ar-20% Methane and operate in the TPC pressure volume at 8.5 atm. Furthermore, unlike streamer and Geiger modes, the proportional mode is non-saturating in its energy response, and thereby maintains a square-root improvement in energy resolution up to energies where leakage fluctuations become significant.

### A. Model A Prototype.

The first module consisted of a stack of Pb-stainless steel laminates, with wire planes between each laminate. The avalanche wires were stainless steel 20-micron diameter wires spaced every 1.1 cm, and secured by solder and a subsequent epoxy joint to a G10 frame. The laminates were required to be both structurally rigid and to have a good electrical surface, and consisted of

| Material | Depth (ins) | Rad. Length |
|---|---|---|
| Gas Gap | .133" | .0 |
| Laminate: | | |
| Stainless Steel skins | .024" | .0338 |
| Epoxy | .015" | .0012 |
| Pb | .064" | .2892 |
| Per Laminate | .236" | .3242 $X_0$ |
| 54 Laminates | 32.37" | 17.51 $X_0$ |

The module was divided electronically into three sections in depth: in the front section the wires were ganged one wire per gap for 18 gaps, while in the back two sections the wires were ganged two per gap for 18 gaps. Thus the transverse cell size is 1.1 cm in the front section, and 2.2 cm in the back two sections. Each wire frame had 16 wires, so the width of the sensitive area was 17.6 cm.

Both calorimeter modules and their associated beam lines were simulated in detail using the EGS Code[2] as a base. For the beam line, all material downstream of the last momentum-defining slit was included, beam electrons were allowed to shower in the beam line material, and the correct trigger conditions were imposed for each incident electron. Thus the spatial extent of the beam in the module was correctly reproduced, and furthermore, the correct incident energy distribution of electromagnetic particles was correctly simulated even for those beam electrons which began to shower in the beam line upstream of the module, but nevertheless satisfied the trigger in spite of a halo veto requirement. For our purposes in studying gaseous calorimeters, we have augmented the EGS code by performing the transport and energy loss processes in the gas down to electron kinetic energies of a few keV. The EGS code was allowed to follow shower electrons down to a kinetic energy of Tcut=1.0 MeV in a calorimeter with vacuum gaps. A shower electron passing through the gap is gaussian multiple scattered in 1-mm steps, and the ionization and excitation in the gas medium is calculated using the method of Ispirian et al.[3] Each delta-ray generated by this method loses a fraction of its energy in the gas calculated from a range-energy relationship at these energies[4]; a cut is made on the delta-ray range

of 7.5 gaps widths, equivalent to an energy cut of 200 keV at 10 atm. All such gas energy deposits are collected on the nearest proportional wire and weighted by both a measured charge collection efficiency[5] in the gap, and a fixed wire gain factor for this particular wire chosen from a measured distribution[6] of wire gains. These wire signals are ganged into the appropriate electronic channel and written to tape in the same format as the data, and all analyses are performed by the same program.[7]

Each channel was calibrated by depositing a known amount of charge on each channel through a coupling capacitor mounted on the G10 frame, and recording the response of the electronic system to this known charge. The electronic signals in all channels were corrected for temperature and pressure variations during the data taking using the experimentally measured factor of about 9.0 relating the fractional variation in gain to the fractional variation in gas density.

Model A was exposed to the SLAC C-beam at electron energies of 0.25, 0.5, 1.0, 2.0, 4.0, 8.0, and 12.0 GeV at a pressure of 10.2 atm, and at 1.0 GeV for pressures of 1.0, 1.7, 3.0, 5.8, 10.2, 15.1, 22.1, and 29.9 atms. The gas mixture in this test was 90% Ar-10% Methane.

The resulting pulse height distributions were fitted to a gaussian form, excluding the data beyond 2 standard deviations of the fitted mean. The resulting rms energy resolutions are displayed in Table 1 for the energy scan, and in Table 2 for the pressure scan.

Table 1. Model A energy resolution at P=10.2 atm, versus electron energy.

| | $\sqrt{E}(\sigma/E)$ $(GeV^{1/2})$ | |
|---|---|---|
| E(GeV) | Data | Simulation |
| .25 | 14.9 ± 0.5% | 13.4 ± 0.3% |
| .50 | 13.9 ± 0.3% | 14.0 ± 0.3% |
| 1.0 | 14.4 ± 0.2% | 14.6 ± 0.3% |
| 2.0 | 13.5 ± 0.2% | 14.6 ± 0.3% |
| 4.0 | 14.6 ± 0.2% | 14.2 ± 0.4% |
| 8.0 | 15.2 ± 0.2% | 15.3 ± 0.5% |
| 12.0 | 15.7 ± 0.4% | 15.5 ± 0.6% |

The pulse height distributions at all energies are shown in Figure 1.

Table 2. Model A energy resolution at E=1.0 GeV versus gas pressure.

| | $\sqrt{E}(\sigma/E)$ $(GeV^{1/2})$ | |
|---|---|---|
| P(atm) | Data | Simulation |
| 1.0 | 16.4 ± 0.6% | 17.9 ± 0.2% |
| 1.7 | 17.1 ± 0.3% | 17.0 ± 0.2% |
| 3.0 | 16.8 ± 0.3% | 15.6 ± 0.2% |
| 5.8 | 15.1 ± 0.3% | 15.1 ± 0.2% |
| 10.2 | 14.3 ± 0.1% | 14.5 ± 0.2% |
| 15.1 | 14.2 ± 0.2% | 13.2 ± 0.2% |
| 22.1 | 13.8 ± 0.2% | 12.9 ± 0.2% |
| 29.9 | 13.5 ± 0.4% | 12.4 ± 0.1% |

In the simulation, we have in addition accumulated distributions for the component physical processes which make up the final overall measured resolution. Thus, the distribution of the number of shower tracks per trigger, the distribution of the total pathlength of electrons in the gas gaps, the distribution of the total Landau energy deposit in the gas, and finally the gain corrected energy deposits are accumulated. The distribution of the number of shower tracks is governed largely by the radiator thickness, the total pathlength is in

addition strongly influenced by the low energy electron track angle obliquity distribution, and lastly the energy deposit distribution is affected by the details of the Landau distribution for this particular gas. We display in Fig. 2 each of these components as they contribute in turn at the overall energy resolution.

The depth development of the shower in the three electronic depth sections was in good agreement with the simulation, although discrepancies of the order of a few percent are evident. The distribution functions of the energy deposited in the three sections for both Model A data and simulation are shown in Fig. 3 for 2 GeV showers. Other energies are equally good.

B. Model B Calorimeter.

The second module was designed to be as close as possible to the final full scale Pole Tip configuration, and in addition was tested both with and without a B=10 kgauss magnetic field along the shower axis. The laminate fabrication for Model B was

| Material | Depth (ins) | Rad. Length |
|---|---|---|
| Gas Gap | .160" | .0 |
| Laminate (First Section): | | |
| Al Skins | .020" | .0058 $X_0$ |
| Epoxy | .010" | .0008 |
| Pb | .051" | .2304 |
| No. of Laminates: 37 | 8.92" | 8.77 $X_0$ |
| Laminate (Second Section): | | |
| Al Skins | .020" | .0058 |
| Epoxy | .010" | .0008 |
| Pb | .102" | .4607 |
| No. of Laminates: 12 | 3.50" | 5.60 $X_0$ |
| Total | 12.42" | 14.38 X0 |

In Model B, the calorimeter was divided electronically into two depth sections, again one wire per gap for 37 gaps, and two wires per gap for the remaining 12 gaps. The wire spacing was also 1.1 cm, and the sensitive width 17.6 cm. Alternate wire planes were rotated 90 degrees to measure x- and y-coordinates, and in addition, Model B was instrumented with a precision MWPC at its entrance window in order to measure the spatial position of the incident electron for purposes of detailed studies of the shower width and of the distribution function of the deposited energy in nearby channels. The effective wire spacing of this MWPC was 1.0 mm, and it was aligned with the x-coordinate of the calorimeter wire plane. The Pb thickness was doubled in the section depth section to improve the energy resolution at higher energies by reducing leakage.

Model B was exposed to the SLAC C-beam at electron energies of 0.25, 0.5, 0.8, 1.0, 2.0, 4.0, and 8.0 GeV at a pressure of P=10 atm, and at an energy of 1.0 GeV for pressures of 1.0, 2.0, 5.0, and 10. atms. Gaussian fits to the pulse height spectra yielded the results in Table 3 for the energy scan in Model B.

Table 3. Model B energy resolution at P=10 atm. versus electron energy; B = 0 kgauss.

| | $\sqrt{E}(\sigma/E)$ $(GeV^{1/2})$ | |
|---|---|---|
| E(GeV) | Data | Simulation |
| .25 | 10.7 ± 0.2% | 11.6 ± 0.4% |
| .50 | 11.7 ± 0.2% | 11.8 ± 0.4% |
| .80 | 12.1 ± 0.3% | 12.0 ± 0.4% |
| 1.0 | 12.0 ± 0.2% | 12.3 ± 0.4% |
| 2.0 | 12.9 ± 0.2% | 13.3 ± 0.4% |
| 4.0 | 13.1 ± 0.2% | 12.6 ± 0.4% |
| 8.0 | 15.5 ± 0.2% | 15.0 ± 0.5% |

Again, the same simulation program agrees quite well with the measurements in Mobel B.

At lower energies shower maximum is sampled by the thinner plates in the first section of Model B, and leakage fluctuations do not degrade the overall resolution in either calorimeter. At these energies we can compare the resolutions at the same energy and the same radiator thickness.

| | $\sqrt{\frac{E(GeV)}{t(X_0)}}\ \left(\frac{\sigma}{E}\right)$ |
|---|---|
| Model A | 25.3 ± 0.5% |
| Model B | 24.4 ± 0.4% |

Model B was also used for studies of the lateral spread of the electron cascade. For our purposes here, we define the width, W, of a shower as the distance containing the central 50% of the deposited energy in one projection in the front section, a depth of 8.77 $X_0$. These measured widths as a function of shower energy in Model B are listed in Table 4.

Table 4. 50% containment widths in Model B as a function of incident electron energy; B=0 kgauss.

| | W(cm) | | | | | |
|---|---|---|---|---|---|---|
| E(GeV) | Data | Simulation vs. (Tcut+$m_ec^2$)(MeV) | | | | |
| | | 0.6 | 1.5 | 5.0 | 10. | 20. |
| .25 | 1.50 ± .10 | | | | | |
| .50 | 1.60 ± .10 | | | | | |
| 1.0 | 1.40 ± .07 | | | | | |
| 2.0 | 1.19 ± .03 | 1.06±.1 | .80±.1 | .58±.1 | .40±.1 | .28±.1 |
| 4.0 | 1.08 ± .03 | | | | | |
| 8.0 | 1.08 ± .02 | | | | | |

We found that the simulated shower width was strongly dependent on both the low energy cut in the EGS program and on the detailed treatment of delta-rays produced in the gas gap. We varied the EGS Tcut from 0.1 MeV to 20 MeV, and performed two treatments of the delta-rays. In the first, the delta-rays produced by the Ispirian, et al. method in the gas gaps had their energy deposited at their production point; we refer to this as "local". In the second, the produced delta-rays are propagated perpendicular to the shower track, and the whole of their energy deposited at the end of their range if the delta-ray should stop in the gas, or the correct fraction of the energy deposited put into the gas if the delta-ray will bury itself into a laminate; this we refer to as "propagated". In Table 5 we show the results of the four combinations of these treatments at a shower energy of 2 GeV, where the measured width is 1.19 ± .03 cm.

Table 5. Shower width as a function of delta-ray treatment at 2 GeV; B=0 kgauss.

| Condition | Width (cm) |
|---|---|
| Measured | 1.19 ± .03 |
| Tcut=1.0 MeV; Local | 0.78 ± 0.10 |
| Tcut=1.0 MeV; Prop. | 0.80 ± 0.10 |
| Tcut=0.1 MeV; Local | 0.94 ± 0.10 |
| Tcut=0.1 MeV; Prop. | 1.06 ± 0.10 |

In addition, the width as a function of Tcut is shown in Fig. 4 for propagated delta-rays. It is evident that the shower width is dominated by the low energy particles of the shower, as expected, and that good agreement is only obtained by detailed and CPU costly low energy particle treatments.

The integral of the transverse energy deposit for both data and the simulation at 2 GeV are shown in Fig. 5 for the case with Tcut=0.1 MeV and with the delta-ray propagation treatment. Typically, the effect of the magnetic field is to reduce the shower width by about 10% at all energies.

C. PEP Performance.

The full scale Pole Tip calorimeters, similar in configuration to Model B, have been operating for several months in the PEP beams. At a beam energy of 14.5 GeV, the energy resolution in the calorimeters is 5.2%, whereas the EGS calculation gives 4.3%. These resolutions are obtained without attempts to improve the resolution by estimating the leakage energy for each shower, and are therefore upper limits on the energy resolution. The distribution is shown in Fig. 6.

The geometry of the Pole Tip calorimeters has three stereo views at 60 degrees with respect to each other. In each view the centroid of the shower may be estimated by finding the point at which the integeral curve of Fig. 5 crosses 50%; this is just the median of the energy deposited in that view. There are three spatial intersections of these three views, and an analysis of Bhabha events has determined that the spatial resolution at 14.5 GeV shower energy is 1.6 mm at the face of the calorimeter, or 1.3 mrad in this calorimeter with a channel granularity of 8.5 mrad.

## References

1. W. Wenzel, "Geiger Mode Calorimeter", presented at this Workshop.
2. The EGS Code System: Computer Programs for the Monte Carlo Simulation of Electromagnetic Cascade Showers (Version 3), SLAC-210, June 1978, R. L. Ford and W. R. Nelson.
3. K. A. Ispirian, et al., NIM 117 (1974) 125.
4. E. J. Kobetich, et al., PR 170 (1978) 391.
5. R. Koda, UCLA HEE-156, 7 Jan. 1981.
6. J. Hauptman, UCLA HEE-100, 5 Oct. 1978.
7. J. Kubic, UCLA HEE-158, 2 Feb. 1981.

## Figure Captions

Figure 1. The histograms are summed pulse height distributions at energies of 0.25, 0.5, 1.0, 2.0, 4.0, 8.0, and 12.0 GeV for incident electrons in the Model A calorimeter. The horizontal axis is the square root of the beam energy, so that all distributions have roughly the same width. The overlaid points are the results of the simulation described in the text.

Figure 2. The components of the overall energy resolution as calculated in the simulation, as a function of the gas pressure in Model A. The "track counting" curve is the rms percent variation in the number of shower tracks, and is essentially pressure-independent. The "multiple scattering" curve is the rms variation in the pathlengths of shower tracks within the gas gaps. The "MS+Landau" curve includes the Landau distribution on each shower track in the gap, and finally, the "MS+Landau+wires" curve includes the effects of charge collection efficiency and wire gain variations, both meaured for Model A.

Figure 3. The distribution function of the energy deposited in the three depth sections of Model A. The histograms are the data, and the points are the results of the simulation.

Figure 4. The shower width as a function of the kinetic energy cutoff, Tcut, in the simulation, compared to the data at E = 2 GeV.

Figure 5. The measured integral of the transverse shower distribution function, normalized to 1. The open circles are the results of the simulation, and the solid circles are the data.

Figure 6. The summed pulse height response function of the full scale Pole Tip calorimeters to Bhabha scattering events at 14.5 GeV at PEP. The low side tail on the distribution is due to radiative effects.

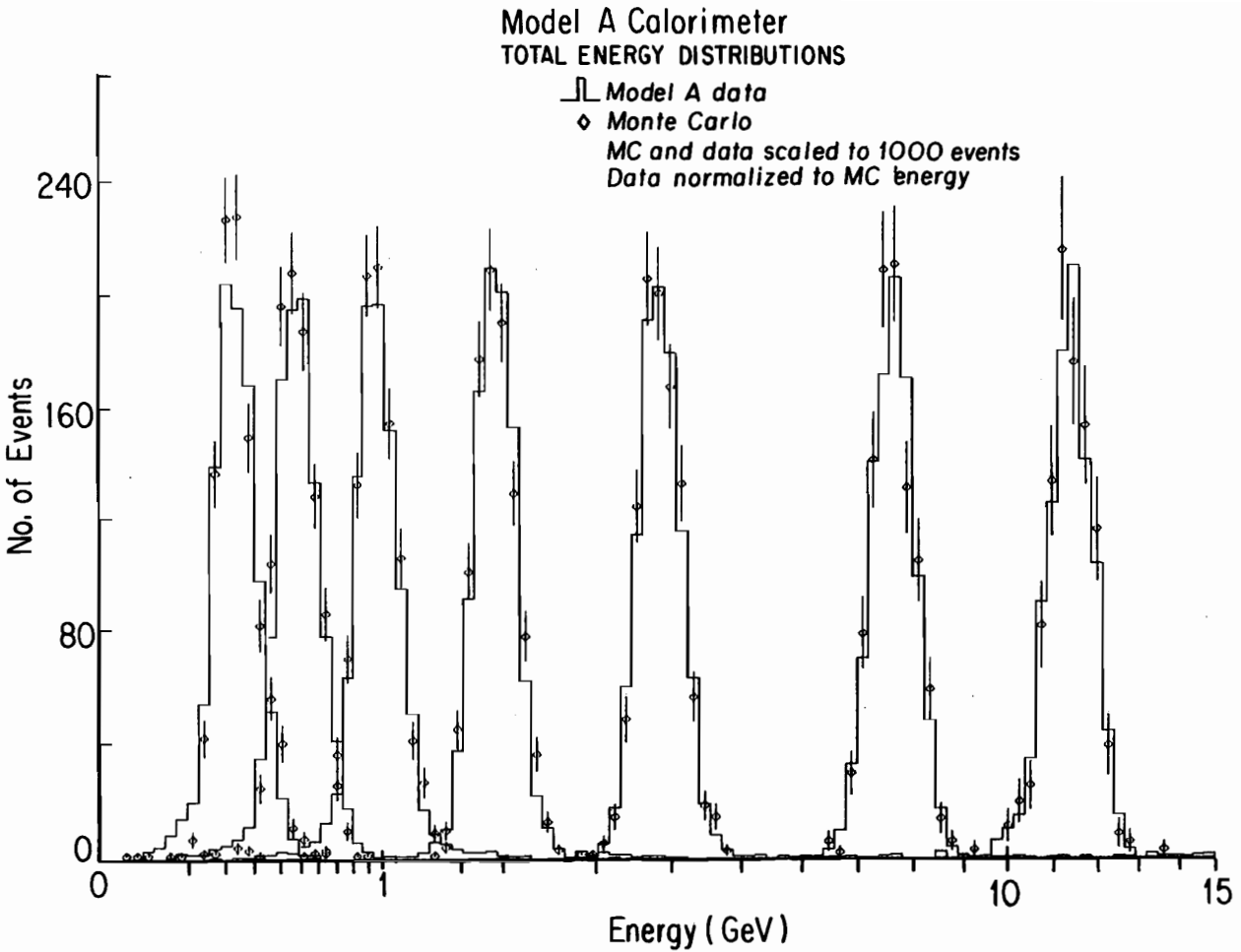
Model A Calorimeter
TOTAL ENERGY DISTRIBUTIONS
Model A data
Monte Carlo
MC and data scaled to 1000 events
Data normalized to MC energy
No. of Events
240
160
80
0
0
1
10
15
Energy ( GeV )

Fig. 1

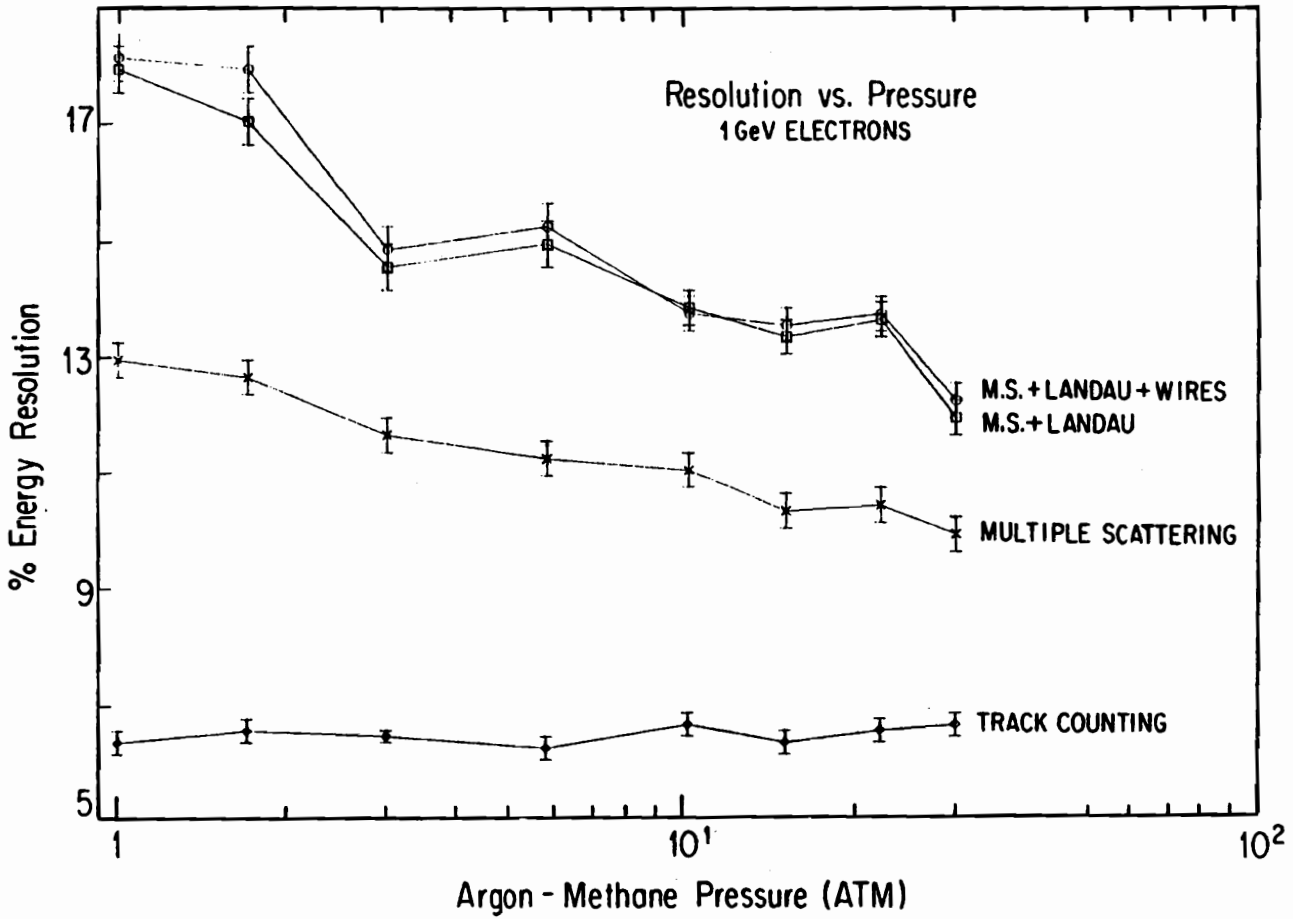
Resolution vs. Pressure
1 GeV ELECTRONS
% Energy Resolution
17
13
9
5
1
$10^1$
$10^2$
Argon - Methane Pressure (ATM)
M.S. + LANDAU + WIRES
M.S. + LANDAU
MULTIPLE SCATTERING
TRACK COUNTING

Fig. 2

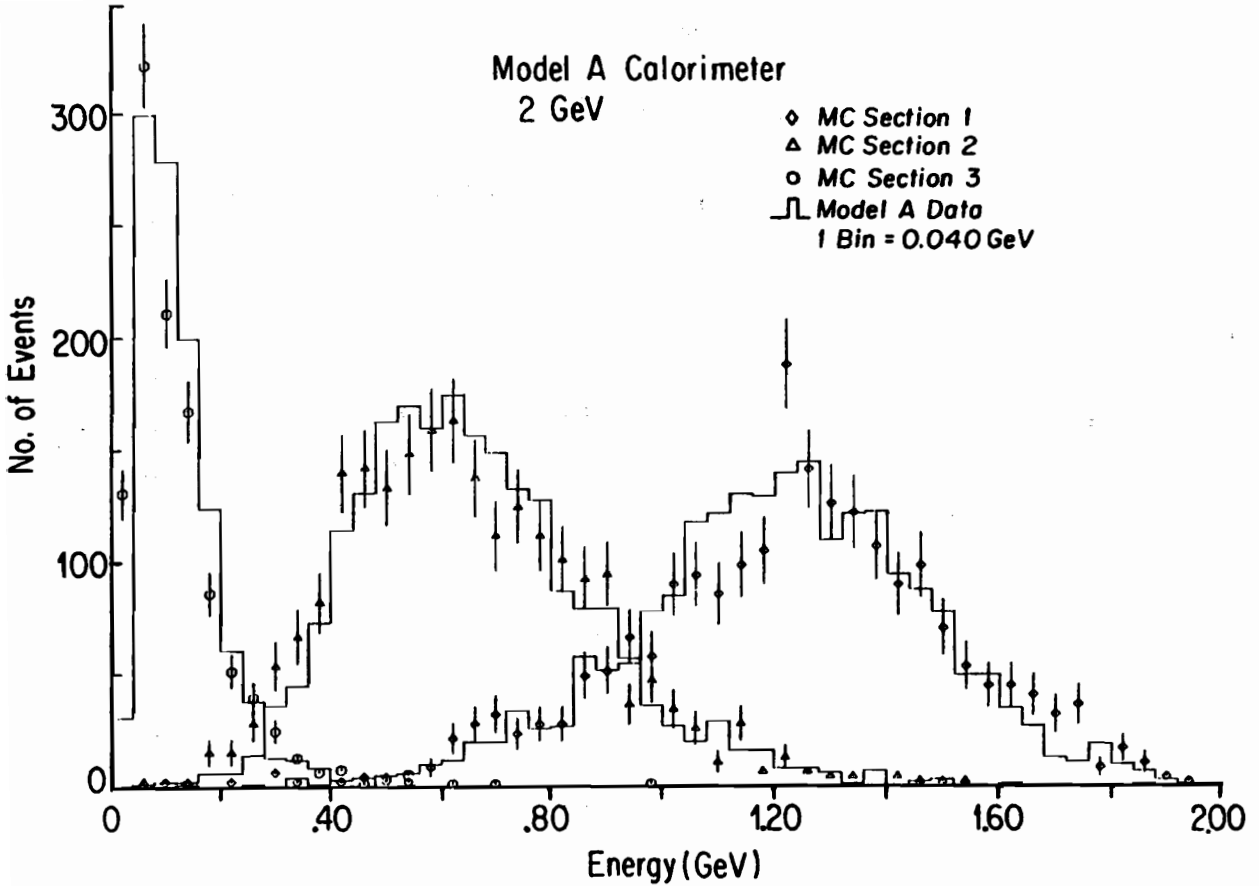
Model A Calorimeter
2 GeV
MC Section 1
MC Section 2
MC Section 3
Model A Data
1 Bin = 0.040 GeV
No. of Events
300
200
100
0
0
.40
.80
1.20
1.60
2.00
Energy (GeV)

Fig. 3

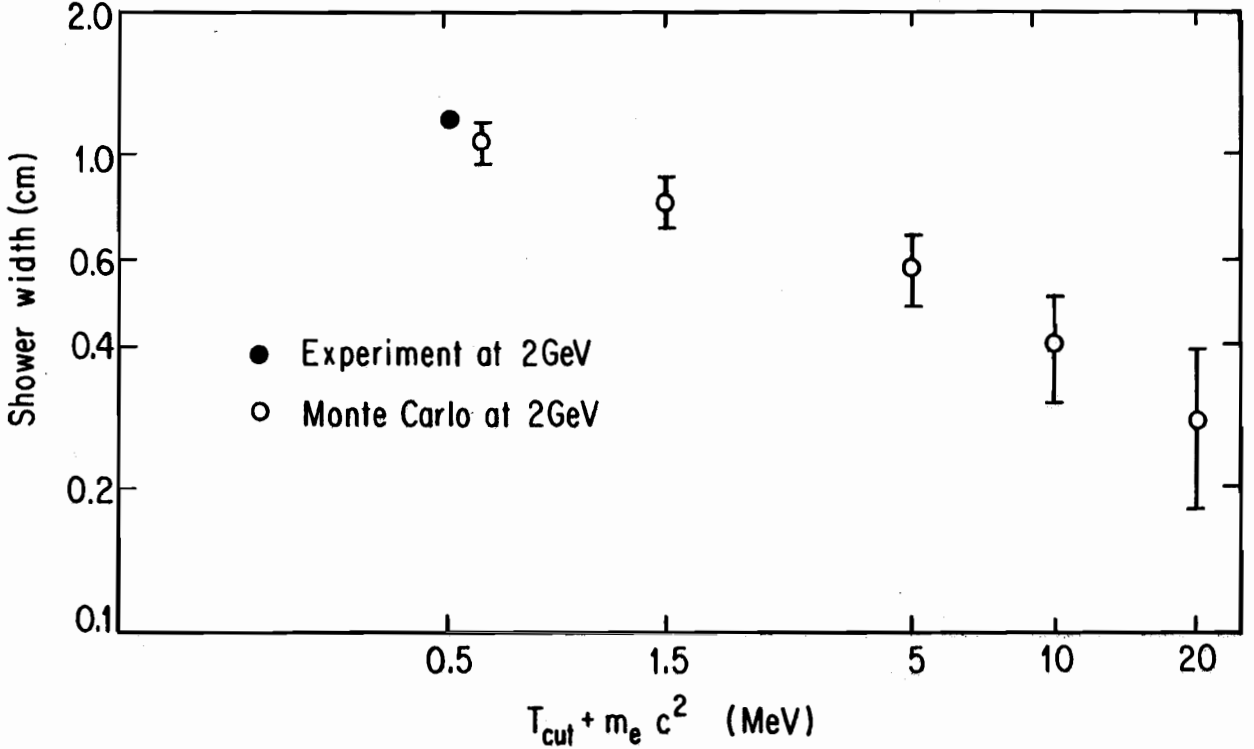
2.0
1.0
0.6
0.4
0.2
0.1
Shower width (cm)
Experiment at 2GeV
Monte Carlo at 2GeV
0.5
1.5
5
10
20
$T_{cut} + m_e c^2$ (MeV)

Fig. 4

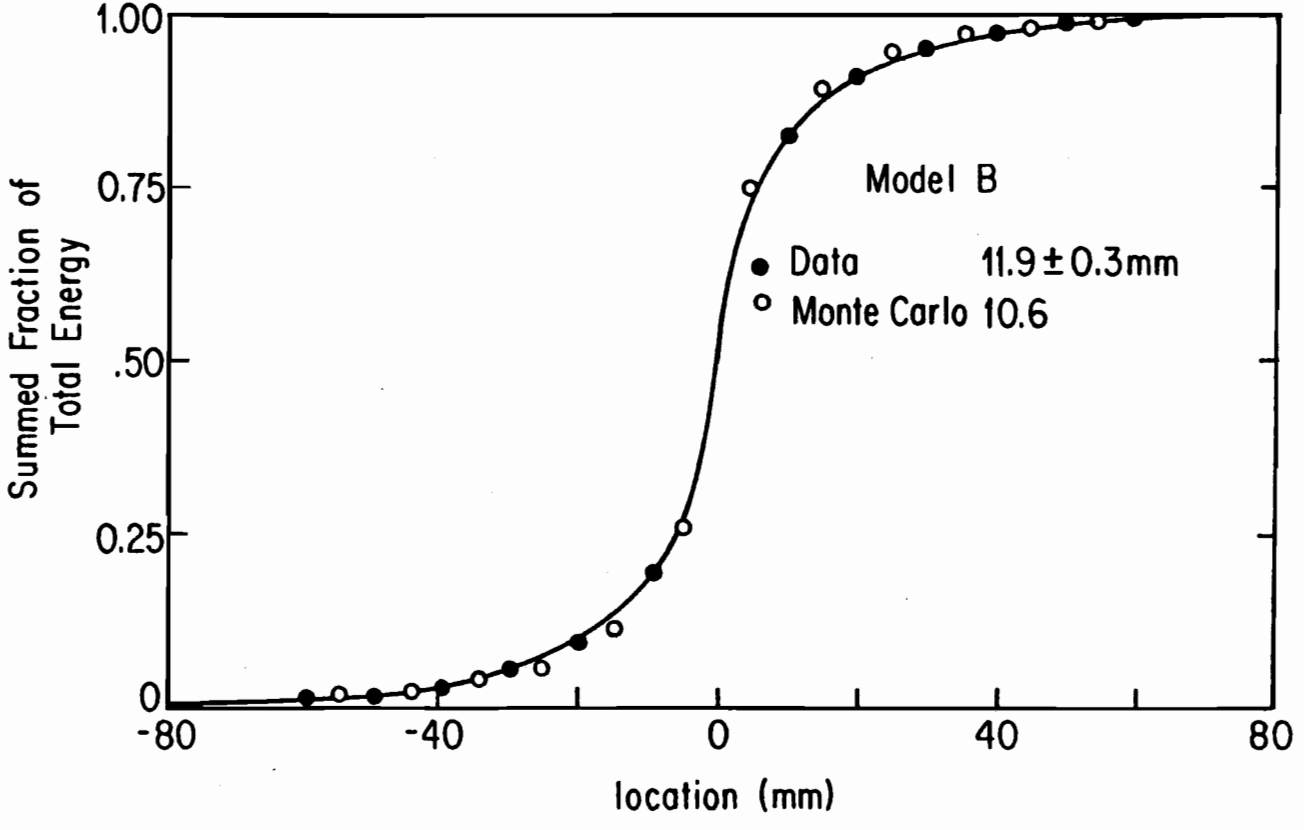
1.00
0.75
.50
0.25
0
Summed Fraction of Total Energy
-80
-40
0
40
80
location (mm)
Model B
Data
11.9 ± 0.3mm
Monte Carlo 10.6

Fig. 5

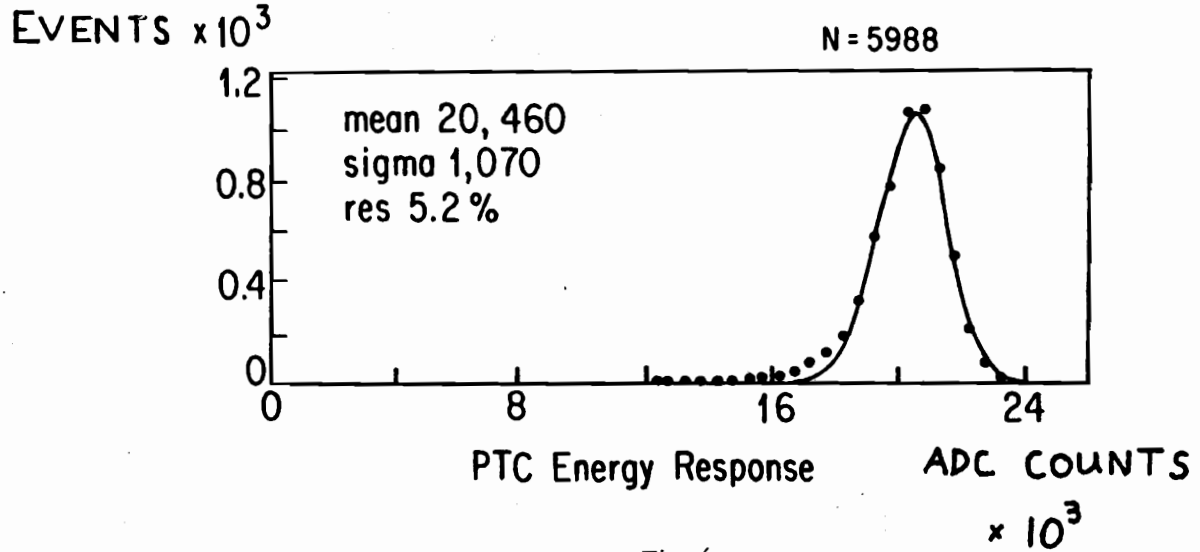
EVENTS x 10^3
N = 5988
1.2
0.8
0.4
0
mean 20, 460
sigma 1,070
res 5.2 %
0
8
16
24
PTC Energy Response
ADC COUNTS
x 10^3

Fig. 6